Optimizing performance of metamaterial wormhole superabsorbers

Hugo R. L. Ferreira ⊙

Instituto de Telecomunicações, DEEC FCTUC Pólo II-Pinhal de Marrocos 3030–290 Coimbra, Portugal

Nuno G. B. Brás ⊙

Instituto de Telecomunicações, Instituto Superior Técnico, Av. Rovisco Pais 1 1049–001 Lisboa, Portugal,
and Universidade Autónoma de Lisboa Rua Santa Marta 56–Palácio Dos Condes Do Redondo 1169-023 Lisboa, Portugal

Stanislav I. Maslovski ⊙*

Instituto de Telecomunicações e Departamento de Eletrónica, Telecomunicações e Informática Universidade de Aveiro
Campus Universitário de Santiago 3810-193 Aveiro, Portugal

Transmission line-based metamaterials are used to realize and model the conjugate-impedance matched superabsorbers. Here, we formulate an analytical-numerical approach for maximizing the effective absorption cross section of the metamaterial wormhole superabsorber, under the goal of minimizing the complexity of the structure. Analytical expressions for the gradient of the absorption cross section as a function of the structural parameters are derived. Numerical results showing enhanced absorption are obtained under three different optimization strategies: a ring-by-ring approach, a gradient-based optimization, and a mixed algorithm. The best results are achieved with the mixed algorithm, with which it is demonstrated that the optimal wormhole superabsorber significantly outperforms a black body-type absorber of a similar size. This study is of a particular interest for applications of the conjugate-impedance-matched superabsorbers as efficient harvesters of electromagnetic radiation.

I. INTRODUCTION

As is well known, resonant objects such as plasmonic nanoparticles may have scattering and absorption cross sections much greater than those of nonresonant objects with the same geometric dimensions [1]. For instance, the extinction cross section in subwavelength particles exhibiting plasmonic or polaritonic resonances can be many orders of magnitude larger as compared to a black-body absorber of similar physical size [2–9]. Effectively, such resonant particles are able to collect the incident wave power from an area much bigger than the physical size of the particles.

By realizing the necessary conjugate-impedance match condition between every spatial harmonic of an incident wave with a given frequency and a finite-size body, one can show that there is no upper limit on the effective absorption cross section of such a body (at a selected wavelength), even when the body is large as compared to the wavelength. Such finite-size superabsorbers [10–13], which can be realized with metamaterials [14], exhibit peculiar behavior when interacting with passing electromagnetic waves [15].

The present work deals with one of such superabsorber realizations. Although this work focuses mainly on the optimization of absorption by a specific conjugate-impedance matched object that we call "metamaterial wormhole," it has wider physical implications. Namely, this work is a follow-up of Ref. [16], where we proposed a way of physical modeling

of conjugate-impedance matched superabsorbers [11]. Such objects posses unique physical properties, for example, they allow for free-space super-Planckian thermal emission [12].

A particularly exotic object—"metamaterial thermal black hole"—formed by a medium with simultaneously negative permittivity and permeability [17] can be constructed [12] to posses, theoretically, arbitrarily large absorption cross section at a given wavelength, independently of the physical dimensions of the object. In practice, the performance of such superabsorbers is limited to a narrow frequency band close to the resonant frequency, at which the conjugate-impedance match condition is satisfied [12]. Numerical modeling of such objects in order to identify the performance limits imposed, e.g., by the dissipation and granularity of the metamaterials, can be seen as a prerequisite for first experimental realizations of such superabsorbers and superemitters.

In the previous work [16] we proposed to model the above-mentioned objects and the related wave phenomena in quasi-two-dimensional (quasi-2D) configuration, by using a topological analogy between a metamaterial thermal black hole in n-dimensional space and an equivalent wormhole structure in $(n + 1)$-dimensional space. Such physical model preserves the main wave scattering and absorption effects associated with the metamaterial thermal black holes and, at the same time, reduces the complexity of the involved metamaterials. In particular, the so-called transmission line-based metamaterials can be employed [18–20].

It has to be mentioned that the "black hole" and "wormhole" terminology that we use here does not imply a direct

---

*Corresponding author: stas@av.it.pt

analogy with the light propagation in a vicinity of similarly named cellestial objects. However, a few related effects reported previously, such as the trapping of passing beams of radiation and the full absorption of incident light, have resulted in a wide acceptance of such terminology in the literature [21–24], especially when dealing with metamaterial structures realized with the transformation optics techniques [25].

In Ref. [16], the superabsorption effect was demonstrated in a uniform wormhole structure formed by dual meshes of loaded transmission lines (TL) realizing the double-positive (DPS) and double-negative (DNG) metamaterials. Theoretical analysis of such a structure was carried out based on the developed analytical model. In the same work, an alternative realization dealing with rings of DNG unit cells with varying parameters (the characteristic impedance, the electrical length, etc.) was proposed, motivated by an observation that, for optically large objects, the required number of the DNG cells in the wormhole superabsorber can become too high, which forbids any practical realization. Therefore, it is necessary to consider alternative realizations, which allow for a significant reduction in the number of the DNG cells, while attaining a comparable performance.

As was pointed out already in Ref. [16], achieving this goal would require formulating and solving a global numerical optimization problem involving sophisticated optimization techniques. While an attempt on optimizing the parameters of every single DNG cell in the system is imaginable, it is impractical with moderate hardware due to a huge number of optimization variables. Therefore, in our approach, we sort the DNG cells in the system into uniform concentric rings, and optimize the cell parameters per each ring. In this article, we extend the initial results presented in Ref. [16] by developing global gradient- and exhaustive search-based optimization techniques, with the goal of optimizing the model parameters and maximizing the absorption cross section of the wormhole object, while keeping the structural complexity at a reasonably low level.

This article is structured as follows. In Sec. II, we discuss the mathematical model of the wormhole superabsorber and derive explicit formulas for the gradient of the absorption cross section with respect to some model parameters. In Sec. III we detail the optimization algorithms used in this work and discuss the numerical results obtained under different optimization strategies. Finally, in Sec. IV the main conclusions of this work are drawn.

II. PROBLEM FORMULATION

The geometry of the superabsorbing wormhole structure is shown in Fig. 1. The structure comprises TL-based metamaterials (i.e., meshes of loaded transmission lines) of two different types: DPS and DNG. In Fig. 1, most of the top plane is formed by the DPS metamaterial that has positive effective permeability and permittivity at the frequency of operation. The wormhole object in the middle of the structure connects the two planes and is formed by a DNG metamaterial, in which the effective material constants are both negative. Further details on the unit cell realizations of the DPS and DNG meshes can be found in Ref. [16].

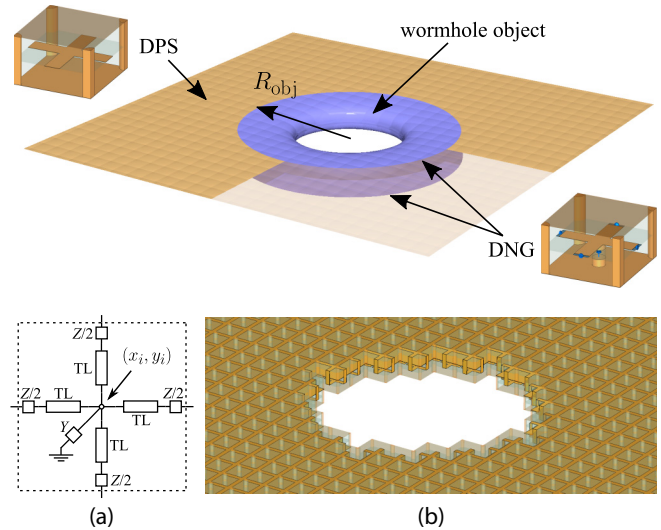The software realization of the frequency domain transmission line matrix (FDTLM, [26,27]) model detailed in

FIG. 1. Top: The geometry of the superabsorbing metamaterial wormhole object. The structure is formed by meshes of transmission lines: A mesh with double-positive (DPS) and a mesh with double-negative (DNG) effective material parameters. The wormhole object with radius $R_{\rm obj}$ in the middle of the structure is composed of the DNG mesh. The DPS mesh is electrically connected to the DNG mesh that continues through the wormhole. In this figure, one quarter of the DPS mesh is made semi-transparent in order to make the underlying structure visible. The structure of the DPS and DNG unit cells [16] is also shown. Bottom: Equivalent circuit of the DNG unit cell (a) and a zoom-in picture showing the connections between the unit cells in the top and the bottom planes in the wormhole region (b), as in Ref. [16].

Ref. [16] had allowed us to perform a number of studies on the interaction of the wormhole superabsorber with the waves propagating in the DPS and DNG domains. In Ref. [16], we presented results demonstrating enhanced absorption of plane waves and trapping of Gaussian beams under a number of quasi-2D excitation scenarios. The achieved performance gain, as compared to the reference black body case, was about 46% for a wormhole superabsorber comprising about 1.2×10^4 DNG cells characterized by the normalized cell size $\beta_0 d = 0.315$ and the loss tangent parameter $\alpha = 10^{-4}$. The normalized wormhole radius in this case was $\beta_0 R_{\rm wh} = 9.45$. For structures with smaller normalized radii and a comparable number of the DNG cells, the achievable gain can be higher.

For example, the gain of 170% was reported in Ref. [16] for the case with $\beta_0 d = 0.1$ and $\beta_0 R_{\rm wh} = 1.5$. However, in this case, the wormhole's diameter was subwavelength, and it was already well-known that subwavelength absorbers could exhibit performance much greater than what could be estimated based just on their size. Therefore, in the present work, we concentrate on moderately sized wormhole objects with the normalized radii $\beta_0 R_{\rm obj} \approx 10$, i.e., on the objects with circumference on the order of ten wavelength.

As compared to the uniform wormhole structure studied in detail in our previous work [16], the wormhole object located in the middle of the structure shown in Fig. 1 is formed by concentric rings of the DNG cells with varying parameters,

such as the normalized characteristic impedance $Z_0 = Z_c/Z_{ref}$, with Z_{ref} being the TL impedance in the DPS region, and the normalized cell size $\beta_0 d = 2\pi d/\lambda_0$, where d is the size of the square unit cells and λ_0 is the wavelength in the unloaded TL segments. Such a metamaterial wormhole can be used to model a cylindrical conjugate-impedance matched superabsorber [10,11].

The unit cells are sorted into the rings based on the distance from the middle axis of the structure to the cell's center. If this distance, r, falls within the interval $R_{ring} - h < r \leqslant R_{ring}$, where R_{ring} is the outer radius of a given ring and h is the ring width, then the cell is considered as belonging to the ring. In our structure, $h \ll R_{ring}$ and $d \ll R_{ring}$, while $h \geqslant d$.

The goal of the present paper is to look for the optimal geometry and the unit cell parameters of the structure shown in Fig. 1 in order to maximize its effective absorption cross section, σ_{abs}, defined as

$$\sigma_{abs} = \frac{P_{abs}}{\Pi_{inc}}, \tag{1}$$

where Π_{inc} (W/m) measures the power density of the incident plane wave (per unit length, due to the quasi-2D propagation) and P_{abs} (W) is the total power absorbed by the wormhole object. We are interested in the cases when $\sigma_{abs} > 2R_{obj}$, where R_{obj} is the radius of the object, i.e., when the effective absorption cross section exceeds the physical size of the absorber.

The wave scattering and absorption in the structure shown in Fig. 1 can be studied by using the FDTLM method that was employed in our previous work [16]. For the sake of completeness, in Appendix A we give some details of this method that constitutes the theoretical framework used in this article, and which results in the calculation of the effective absorption cross section of the wormhole.

Under this framework, in order to find the wave field (represented by the incident and reflected voltages in the TL mesh) at each point in the structure, one has to solve the following linear system of equations:

$$(\mathbf{I} - \mathbf{CS})\mathbf{V}^{inc} = \mathbf{V}^{ext}. \tag{2}$$

In this system, the matrix $\mathbf{A} = \mathbf{I} - \mathbf{CS}$ relates the the vector of incident voltages in the TL segments, $\mathbf{V}^{inc}$, which are the unknowns of the problem, to the given excitation represented by the vector of external voltages, $\mathbf{V}^{ext}$. Here, $\mathbf{I}$ is the identity matrix, $\mathbf{C}$ is the connection matrix that describes the electrical connections between the unit cells of the structure, and $\mathbf{S} = \text{diag}[\mathbf{S}_{cell,1}, \ldots \mathbf{S}_{cell,N}]$ is a block-diagonal matrix formed by the scattering matrices of the unit cells. This matrix relates the vectors of the incident and reflected voltages in the whole structure: $\mathbf{V}^{ref} = \mathbf{SV}^{inc}$.

Using the FDTLM method, we can find the amount of power entering the wormhole under a quasi-2D plane wave excitation scenario and then express the derivative of the absorption cross section σ_{abs} with respect to some (structural or electric) parameter ρ. This will allow us to obtain an explicit formula for the gradient of the absorption cross section with respect to a set of optimization parameters.

In doing so, starting from Eq. (1), we may write

$$\frac{\partial \sigma_{abs}}{\partial \rho} = \frac{1}{\Pi_{inc}} \frac{\partial P_{abs}}{\partial \rho}. \tag{3}$$

The absorbed power can be expressed as

$$P_{abs} = \frac{1}{2Z_{ref}} \mathbf{V}^{ext\dagger} \mathbf{H} \mathbf{V}^{ext}, \tag{4}$$

where Z_{ref} is the reference impedance, and

$$\mathbf{H}(\rho) = \mathbf{A}(\rho)^{-1\dagger}(\mathbf{DS}(\rho) - \mathbf{S}(\rho)^{\dagger}\mathbf{D})\mathbf{A}(\rho)^{-1}. \tag{5}$$

Here, $\mathbf{D}$ is a matrix that describes the connections of the wormhole object to the uniform DPS region where the incident field propagates (see Appendix A).

By substituting this result into Eq. (3), performing the differentiation, and noting that $\mathbf{V}^{ext\dagger}\mathbf{A}^{-1\dagger} = \mathbf{V}^{inc\dagger}$ and $\mathbf{A}^{-1}\mathbf{V}^{ext} = \mathbf{V}^{inc}$, we obtain an explicit relation between our maximization target (σ_{abs}) and the parameter under study (ρ_i):

$$\frac{\partial \sigma_{abs}}{\partial \rho_i} = \frac{\text{Re}\big[\mathbf{V}^{inc\dagger}(\mathbf{D} - \mathbf{S}^{\dagger}\mathbf{DC})\mathbf{A}^{-1T} \frac{\partial \mathbf{S}}{\partial \rho_i} \mathbf{V}^{inc}\big]}{\Pi_{inc} Z_{ref}}. \tag{6}$$

In this expression, the derivative of the whole scattering matrix $\mathbf{S}$ with respect to the parameter ρ_i associated with a selected unit cell (the ith cell) is $\partial \mathbf{S}/\partial \rho_i = \text{diag}[\mathbf{0}, \ldots \mathbf{0}, (\partial \mathbf{S}_{cell}/\partial \rho_i)_i, \mathbf{0}, \ldots \mathbf{0}]$.

The final step in obtaining a complete set of equations to calculate the gradient of the absorption cross section with respect to some set of parameters $\{\rho_i\}$, is to choose said parameters. In this work we choose the normalized unit cell parameters $\beta_0 d$ and Z_0 as the optimization variables. In terms of these parameters, we find that

$$\frac{\partial \mathbf{S}_{cell}}{\partial Z_0} = -\frac{2}{(Z_0 + 1)^2}(\mathbf{I} + R\mathbf{S}_0)^{-1}(\mathbf{S}_0 \mathbf{S}_{cell} - \mathbf{I}), \tag{7}$$

$$\frac{\partial \mathbf{S}_{cell}}{\partial (\beta_0 d)} = -(\alpha \pm i)(\mathbf{I} + R\mathbf{S}_0)^{-1}\mathbf{S}_0(\mathbf{I} - R\mathbf{S}_{cell}), \tag{8}$$

where $R = (Z_0 - 1)/(Z_0 + 1)$ and $\mathbf{S}_0 = (\frac{1}{2}\mathbf{U} - \mathbf{I})e^{-\beta_0 d(\alpha \pm i)}$ are as defined in Appendix B.

Equations (7) and (8), together with Eq. (6), fully describe the relation between the optimization parameters and the absorption cross section of the wormhole structure. These explicit relations are used in the implementation of faster and more reliable optimization algorithms considered in the following sections.

III. REALIZATION

The numerical model detailed in the previous section involves, as its central point, a sparse matrix inversion. To solve this type of problem there are a number of software libraries available, which are both fast and versatile. In this work we have chosen the SuperLU library [28,29], which performs well and has a well-defined programming interface. The library is programed in C++, but supports interfaces for other programming languages, including Fortran. Both C++ and Fortran have been used in our work to implement the solver for the absorption cross section of the wormhole object with a given set of the cell parameters.

After the forward solver was implemented using the SuperLU library, we focused on implementing the explicit gradient formulation and using it in a number of optimization algorithms to explore the optimization parameter space. In

what follows we shall introduce the various algorithms used to obtain the results presented in this article.

A. Optimization algorithms

The gradient formulation of Sec. II has been employed in the optimization algorithms, which are discussed next, with the goal of identifying the best optimization strategy for the system under study and obtaining the highest value of the absorption cross section. We also include a comparison with the ring-by-ring optimization algorithm first proposed in Ref. [16]. This initial algorithm is a simple exhaustive search in the $\beta_0 d$ and Z_0 parameter space, with an assumption that the optimization of the whole wormhole object can be done by separately optimizing each ring of the DNG cells, independently of the values of $\beta_0 d$ and Z_0 in the other rings. The pseudocode for this and subsequent algorithms are given in Appendix C.

Let us note that straightforward implementations of optimization algorithms that use an explicit gradient function in order to speed up convergence typically operate based on the information obtained from the gradient direction (and, sometimes, value) in order to find the next optimization point. The algorithms of this type work well when the parameter space is smooth. However, a preliminary study has shown that our system is too complex for such a straightforward approach to be successful. Indeed, the structure that we study is assembled by many cells with resonant collective response, which leads to a rather irregular behavior of the target function over the parameter space. The performed calculations have demonstrated that a straightforward implementation of the gradient-based optimization method (such as the well-known gradient descent method) may not work well in our case.

A known variation on this type of methods introduces an additional parameter—momentum (ν)—with which the target function gradient is used in an indirect way, by determining the change in the momentum, which is then used to compute the next point in the parameter space during the optimization. Including such additional variable improves the optimization performance in the complex parameter spaces such as the one that occurs in our study.

This method can be further improved by adding a dumping parameter that may increase the stability of the algorithm. Below we give the update equations for the momentum vector ν and the parameter space vector $\mathbf{x}$ for such an improved algorithm (the index $t = 1, 2, 3, \dots$ enumerates the iterations of the algorithm):

$$\nu_t = \nu_{t-1} + \kappa \nabla \sigma_{\mathrm{abs},t} - \gamma \mathbf{L}(\nu_t, \nabla \sigma_{\mathrm{abs},t}),$$
$$\mathbf{x}_t = \mathbf{x}_{t-1} + \nu_t, \tag{9}$$

where $\mathbf{L}$ is the dumping (or loss) function that, in general, depends on the momentum and the gradient of the target function ($\nabla \sigma_{\mathrm{abs}}$). The parameter γ defines the dumping strength.

In this work we use the loss function which is simply proportional to the momentum: $\mathbf{L}(\nu_t, \nabla \sigma_{\mathrm{abs},t}) = \nu_{t-1}$. Under this assumption, the update equations reduce to

$$\nu_t = (1 - \gamma)\nu_{t-1} + \kappa \nabla \sigma_{\mathrm{abs},t},$$
$$\mathbf{x}_t = \mathbf{x}_{t-1} + \nu_t. \tag{10}$$

Here, the factor $(1 - \gamma)$ represents the fraction of the previous momentum that is considered in the current momentum calculation, and κ is the fraction of the gradient that is taken in consideration at a given step of the algorithm.

The next algorithm that we have implemented and tested is also based on the gradient descent method. However, instead of using it in the whole space of optimization parameters, we use it only in the Z_0 parameter subspace, because, as it has been found by direct calculations, the target function behaves more smoothly in this subspace. For the subspace of $\beta_0 d$ parameters we use an heuristic search method in which the optimal parameter value is determined from an initial setting based on the optimization result obtained by the same algorithm on the previous iteration. For this reason, we refer to it as the mixed algorithm. The details of this algorithm can be found in Appendix C.

Let us note that both the gradient descent and the mixed algorithms can take an initial point in the parameter space as a free parameter. In Sec. III B we explore the consequences of a random initial setting versus using a setting based on the solution obtained for the lower numbers of rings, such as, e.g., using the solution obtained when optimizing the structure with four rings as a starting point for the optimization of the system with five rings, etc.

B. Results

The results of the numerical simulations obtained using the FDTLM method are shown in Fig. 2. We consider a wormhole structure composed of the DPS and the DNG domains, each occupying an area of 120×120 cells (each cell being a square with size $d \times d$). In the shown example, the wormhole has a radius $R_{\mathrm{wh}} = 20d$ and no cells occur in the region where $r < R_{\mathrm{wh}}$ (white space in the figure), such that there is no wave propagation in this area. Instead, a wave propagating in the DPS domain will pass to the DNG domain when reaching the wormhole boundary, through the connections that link the two domains.

The DNG cells that form the object rings in the (mainly) DPS domain are limited to a ring determined by $R_{\mathrm{wh}} < r \leqslant R_{\mathrm{obj}}$, where, for all simulations used in this work, $R_{\mathrm{obj}} = 30d$. This radius sets the upper limit for the radii of the DNG rings that occur in this domain, i.e., in the top plane. In addition, the uniform DNG region in the bottom plane is similarly bounded. So, the number of the object rings in a given simulation can be determined as $N_{\mathrm{rings}} = (R_{\mathrm{obj}} - R_{\mathrm{wh}})/h$, where h is the thickness of each ring. In what follows, $h = d$.

The structure is illuminated by an incident plane wave of unitary amplitude propagating along the y axis. The shadow caused by absorption of the incident wave by the wormhole can be seen in the DPS domain. The diameter of this shadow is greater than the diameter of the object, indicating that the effective absorption cross section is such that

$$\sigma_{\mathrm{norm}} = \frac{\sigma_{\mathrm{abs}}}{2R_{\mathrm{obj}}} > 1, \tag{11}$$

where σ_{norm} is the normalized cross section, which is the characteristic feature of the considered superabsorption effect. To compare, for an ideal black body absorber, $\sigma_{\mathrm{norm}} = 1$.
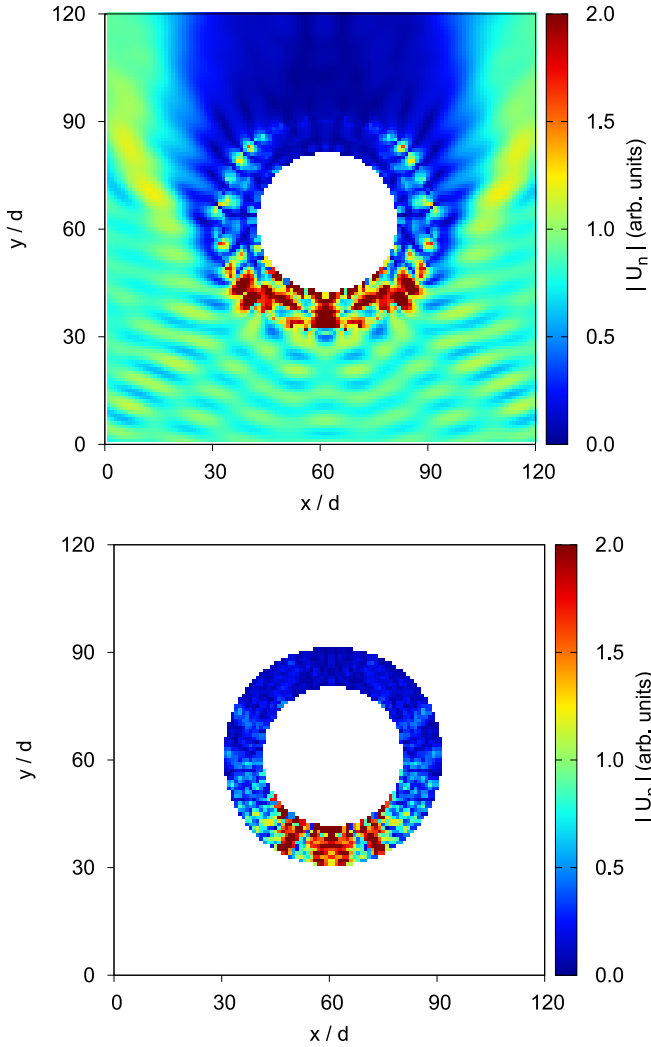
FIG. 2. Distribution of the nodal voltage $|U_n|$, $n = 120[(y/d) + (x/d)] + 1$, $0 \leqslant x/d < 120$, $0 \leqslant y/d < 60$, for the wormhole structure under the plane wave incidence of unitary amplitude, in both the DPS (top) and the DNG (bottom) domains as functions of the normalized coordinates x/d and y/d. The radius of the wormhole is $R_{wh} = 20d$. The fixed parameters of the DPS cells are $\beta_0 d = 0.315$, $Z_0 = 1$, $\alpha = 10^{-4}$. The initial optimization parameters are set based on an optimization attempt with a lower number of the DNG rings.

FIG. 3. Distribution of the nodal voltage $|U_n|$, for the wormhole with radius $R_{wh} = 25d$. Here, the initial optimization parameters are set randomly. The other parameters are as in Fig. 2. The resulting beam in the DNG plane is faint and most energy is reflected off the wormhole, seen as the interference pattern in the DPS plane.

The examples shown in Figs. 2 and 3 demonstrate the difference between the optimized initial setting of the parameters and a random one. By comparing these results it becomes apparent that, for the example shown in Fig. 2, the absorption cross section must be much higher, because much more energy is captured by the wormhole and, respectively, much less is reflected in the DPS plane, as compared to the example of Fig. 3.

Additional simulations (not presented here) show that the structural irregularities that exist due to the mismatch between the shapes of the square unit cells and the circular rings have insignificant influence as compared to the changes in the electrical size of the cells $\beta_0 d$, their impedance Z_0, or the loss parameter α. Such irregularities practically do not affect the maximum attainable value of the absorption cross section,
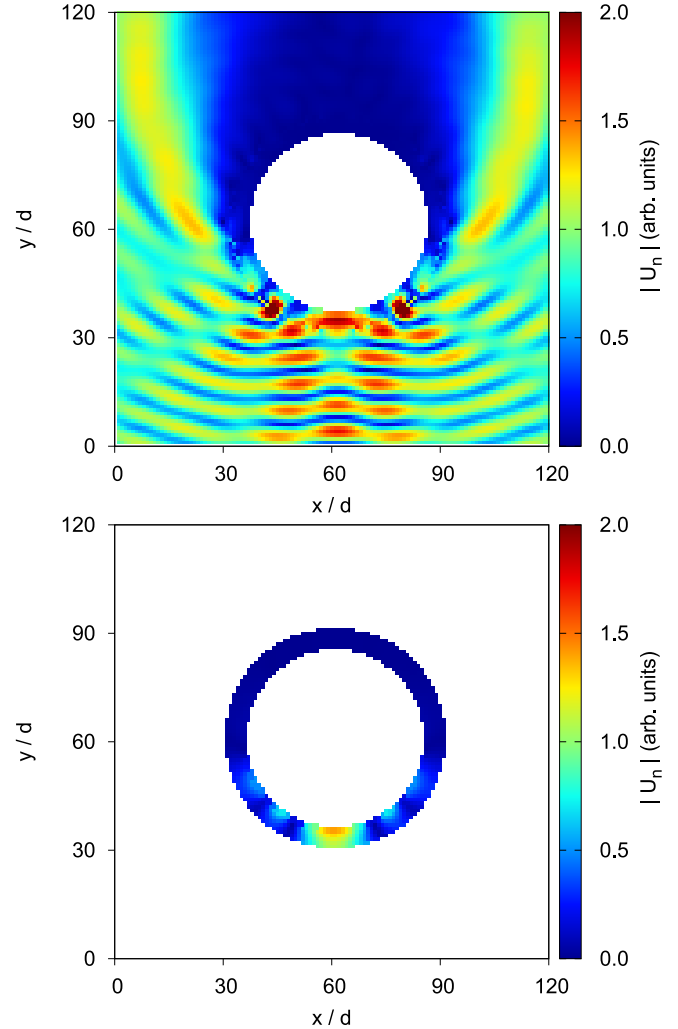
although they do affect the optimal distribution of the $\beta_0 d$ and Z_0 parameters in the nearby rings of cells.

The algorithms with further modifications described in Sec. III A have been used to optimize the wormhole objects with the ring number N_{rings} ranging from 1 to 10. The results for the optimized absorption cross sections are collected in Fig. 4, depicting the maximum σ_{norm} reached by each algorithm as a function of N_{rings}.

From the results depicted in Fig. 4, we can realize a few important details. First, we note that the simple gradient descent approach results in lower σ_{norm} values than the initial ring-by-ring optimization approach, and, even when using the previous solution as the initial point of the optimization, it may only produce results similar to those of the ring-by-ring method. This is due to the high sensitivity of the target function to small variations in any of the selected parameters, which leads to a very inhomogeneous parameter space.

Introduction of the momentum into the gradient descent algorithm has the purpose of smoothing out this
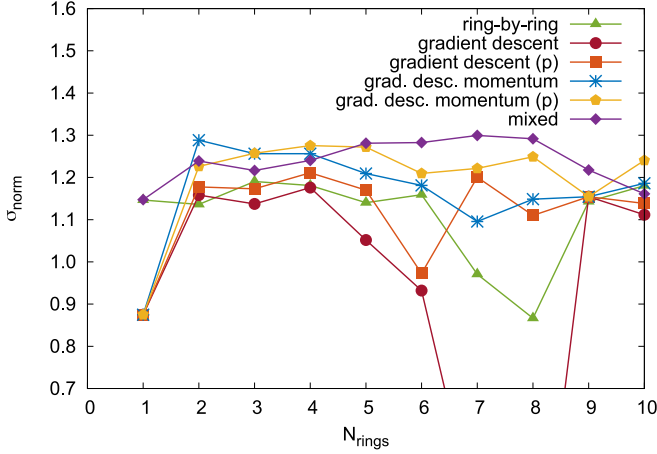
FIG. 4. The maximum obtained σ_{norm} as a function of the total number of rings $N_{\mathrm{rings}} = (R_{\mathrm{obj}} - R_{\mathrm{wh}})/h$. The optimization parameter values have been determined by the optimization algorithms presented in this work. The results of the gradient descent methods with and without the momentum are presented twice: First, using random starting parameters and, second, using the optimized solution for the system composed of $(N_{\mathrm{rings}} - 1)$ rings [marked with "(p)"].

inhomogeneity and obtaining target values that are closer to the global maximum for the considered set of optimization variables. Indeed, we can see a clear improvement in the values of σ_{norm} when the momentum is included. As with the gradient descent method, the initial setting based on the previous optimization step for the structure composed of $(N_{\mathrm{rings}} - 1)$ rings does generally result in a better performance, although in this case the improvement is less pronounced.

Among all optimization approaches that we studied, the mixed algorithm obtains the maximum $\sigma_{\mathrm{norm}} = 1.30$, for the wormhole object with $N_{\mathrm{rings}} = 7$ and the other parameters listed in Table I. Moreover, the mixed algorithm outperforms all other ones in the range $N_{\mathrm{rings}} \in [5, 9]$, where even the gradient descent with momentum cannot navigate the parameter space well. We can conclude that the mixed algorithm performs better, because it uses an exhaustive search for some subset of the optimization parameters and does not rely solely on the values of the local gradients.

The distribution of the field around the object with the optimal structure comprising a rather small number of the

TABLE I. Parameters of the concentric rings of the DNG cells forming the object: The relative outer ring radius r/d, the normalized propagation factor $\beta_0 d$, and the normalized characteristic impedance $Z_0 = Z_c/Z_{\mathrm{ref}}$. These parameters have been obtained using the mixed algorithm, which gives the maximum value of $\sigma_{\mathrm{norm}} = 1.30$ obtained in this work. The last column with $r = 24d$ lists the electrical parameters of the cells in the DNG plane. For the DPS cells the parameters are $(\beta_0 d)^{\mathrm{DPS}} = 0.315$ and $Z_0^{\mathrm{DPS}} = 1$.

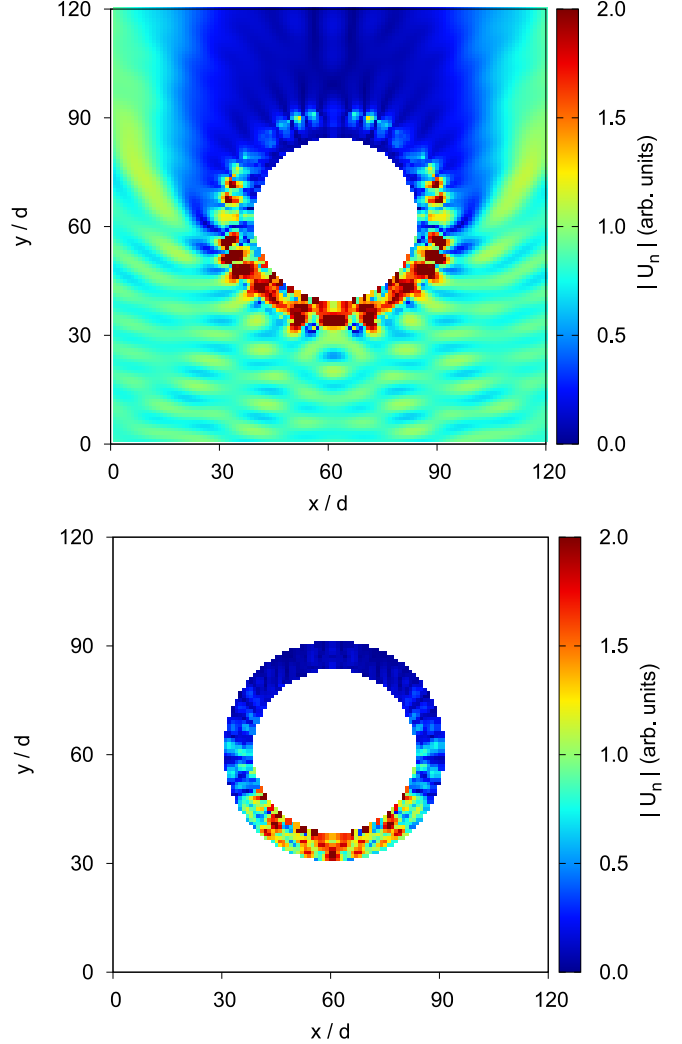| r/d	30	29	28	27	26	25	24
$\beta_0 d$	0.800	1.000	0.200	1.000	0.400	0.365	0.300
Z_0	1.717	2.175	2.082	4.637	2.284	1.549	4.136

FIG. 5. Distribution of nodal voltage $|U_n|$ in the structure with the parameters (listed in Table I) that result in the maximum σ_{norm} value achieved in this work. The wormhole radius is $R_{\mathrm{wh}} = 23d$, and there are seven rings in the wormhole object.

DNG cells is shown in Fig. 5. Despite some reflections which are still present in this setup, the performance of this object is 30% higher than that of a black body absorber with the same diameter. Moreover, such an increase in performance is achieved with a rather small number of the DNG cells distributed around the perimeter of the wormhole.

IV. CONCLUSIONS

In this work, we have studied and optimized superabsorbing metamaterial objects characterized with effective absorption cross sections greater than their physical dimensions. Such objects can be modeled in a quasi-2D propagation environment, by using an equivalent wormhole structure comprising a pair of the DPS and DNG TL-based metamaterial planes.

Interaction of the guided waves in the TL mesh with the wormhole has been studied under the goal of maximizing the effective absorption cross section, while minimizing the

structural complexity. We have extended the original wormhole structure [16] by adding a set of rings formed by the DNG cells into the domain of the DPS cells (the top plane) and reducing the area occupied by the DNG cells in the DNG domain (the bottom plane) to a narrow ring $R_{wh} < r \leqslant R_{obj}$. The electrical size $(\beta_0 d)$ and the characteristic impedance (Z_0) of these rings have been used as the optimization parameters in this work.

We have derived an explicit formulation for the gradient of the absorption cross section as a function of said optimization parameters, and applied it to our system. A number of gradient based optimization strategies have been formulated and compared with the results reported previously [16]. We have discussed the results obtained by these optimization algorithms and selected the best optimization strategy (the mixed gradient-descent/search algorithm) that is most suitable for the rather irregular behavior of the target function over the parameter space that is observed in our system.

The performed optimization has reduced the number of the DNG cells dramatically (from about 1.2×10^4 cells in the original uniform wormhole structure [16] to about 2.3×10^3 in the structure of Fig. 5), while still allowing for the superabsorption effect to occur. With the following parameters of the DPS domain: $(\beta_0 d)^{DPS} = 0.315$, $Z_0^{DPS} = 1$, the loss $\alpha = 10^{-4}$, and the wormhole object of the radius $\beta_0^{DPS} R_{obj} = 9.45$, the maximum normalized absorption cross section has been found to reach $\sigma_{norm} = 1.30$. Thus, we can conclude that even for objects with circumference on the order of 10 wavelengths, optimal wormhole superabsorbers with a greatly reduced complexity (five times smaller number of the DNG cells, as compared to Ref. [16]) can still outperform the black body absorbers by, at least, 30%.

The obtained values of σ_{norm} have to be considered as lower boundary estimates for the global maximum of the absorption cross section in the relevant structures. The main reason of this is that, due to limited computing resources, we do not optimize the parameters of each and every cell separately: Instead we group cells by rings, and perform optimizations on the ring basis. A global cell-based optimization can thus lead to even higher values of the target function.

The superabsorption effect and the considered structures are of interest for potential applications of the superabsorbers as efficient harvesters of electromagnetic radiation, which receive more energy from the incoming radiation than what is falling directly on their surface.

ACKNOWLEDGMENTS

APPENDIX A: NOTES ON FDTLM FORMULATION

We can define a unit cell of our structure as the intersection of two TLs [16]. Here, the scattering parameters for such intersection are calculated based on the normalized size $(\beta_0 d)$ and the normalized characteristic impedance (Z_0) of the unit cell, without considering any particular geometry of the TLs, effectively treating the unit cell as a black box.

These scattering factors form a four-by-four matrix for each cell that relates the incident and reflected wave amplitudes as $\mathbf{V}_{cell}^{ref} = \mathbf{S}_{cell}\mathbf{V}_{cell}^{inc}$. This equation can be extended to the whole structure, with the a block-diagonal scattering matrix $\mathbf{S}$ comprising the individual scattering matrices of each cell of the structure. Each unit cell has connections to the four neighboring nodes. One can define a sparse matrix to represent the connections between the cells, $\mathbf{C}$. In this matrix, the nonzero elements are $\mathbf{C}_{mn} = 1$, where m and n indicate the ports of the neighboring cells that are connected through those ports, implying that $V_m^{inc} = V_n^{ref} + V_m^{ext}$, where V_m^{ext} represents the effect of external sources. The $\mathbf{C}$ matrix is also used to realize the absorbing boundary condition (ABC) at the edges of the structure [16].

In this work we employ an equivalent Huygens source defined in the DPS plane in such a way that, in the absence of the wormhole, the wave solution resulting from the excitation is a plane wave in the region enclosed by the Huygens source boundary. The details on realizing such source can be found in Ref. [16]. The denominator in Eq. (1) is the incident power density due to this source, which is determined by the incident wave amplitude (V_0^{inc}), and is calculated as

$$\Pi_{inc} = \frac{1}{Z_{ref}}(1 - |\Gamma_0|^2)|V_0^{inc}|^2, \tag{A1}$$

where Γ_0 is the Bloch reflection coefficient [16] in the TL mesh.

The total power that enters the wormhole and which is eventually absorbed by the ABCs at the edges of the DNG domain can be expressed as (here we use root-mean-square amplitudes)

$$P_{abs} = \text{Re}\left(\frac{1}{Z_{ref}}\mathbf{V}^{inc\dagger}\mathbf{D}\mathbf{V}^{ref}\right), \tag{A2}$$

where $\mathbf{D}$ is a mask matrix that accounts for the connections at the interface between the DPS and DNG domains, so that the matrix multiplication in Eq. (A2) represents the total power that enters the region of the wormhole absorber. For example, if that interface is right at the circumference of the wormhole, then

$$\mathbf{D} = \begin{pmatrix} \mathbf{0} & -\mathbf{C}_{wh} \\ \mathbf{C}_{wh}^T & \mathbf{0} \end{pmatrix}, \tag{A3}$$

with $\mathbf{C}_{wh}$ defined as the connection matrix that links the top and bottom meshes together [16].

APPENDIX B: EXPLICIT GRADIENT DERIVATION

By differentiating Eq. (5), we obtain the following expression:

$$\begin{aligned}
\frac{\partial \mathbf{H}}{\partial \rho} &= \frac{\partial \mathbf{A}^{-1\dagger}}{\partial \rho}(\mathbf{DS} - \mathbf{S}^\dagger \mathbf{D})\mathbf{A}^{-1} \\
&+ \mathbf{A}^{-1\dagger}\mathbf{D}\frac{\partial \mathbf{S}}{\partial \rho}\mathbf{A}^{-1} - \mathbf{A}^{-1\dagger}\frac{\partial \mathbf{S}^\dagger}{\partial \rho}\mathbf{DA}^{-1} \\
&+ \mathbf{A}^{-1\dagger}(\mathbf{DS} - \mathbf{S}^\dagger \mathbf{D})\frac{\partial \mathbf{A}^{-1}}{\partial \rho}.
\end{aligned} \tag{B1}$$

Considering the following rules for matrix differentiation:

$$\frac{\partial \mathbf{A}^{-1}}{\partial \rho} = -\mathbf{A}^{-1}\frac{\partial \mathbf{A}}{\partial \rho}\mathbf{A}^{-1}, \tag{B2}$$

$$\frac{\partial \mathbf{A}}{\partial \rho} = -\mathbf{C}\frac{\partial \mathbf{S}}{\partial \rho}, \tag{B3}$$

$$\frac{\partial \mathbf{A}^\dagger}{\partial \rho} = -\frac{\partial \mathbf{S}^\dagger}{\partial \rho}\mathbf{C}^\dagger, \tag{B4}$$

and rearranging the terms of Eq. (B1), we obtain

$$\frac{\partial \mathbf{H}}{\partial \rho} = \mathbf{A}^{-1\dagger}\left([\mathbf{D}(\mathbf{I}+\mathbf{S}\mathbf{A}^{-1}\mathbf{C})-\mathbf{S}^\dagger \mathbf{D}\mathbf{A}^{-1}\mathbf{C}]\frac{\partial \mathbf{S}}{\partial \rho}\right)\mathbf{A}^{-1}$$
$$-\mathbf{A}^{-1\dagger}\left(\frac{\partial \mathbf{S}^\dagger}{\partial \rho}[(\mathbf{I}+\mathbf{C}^\dagger \mathbf{A}^{-1\dagger}\mathbf{S}^\dagger)\mathbf{D}-\mathbf{C}^\dagger \mathbf{A}^{-1\dagger}\mathbf{D}\mathbf{S}]\right)\mathbf{A}^{-1}. \tag{B5}$$

We note that the two addends on the right-hand side of Eq. (B5) are conjugate-transpose of each other, therefore, we can work with just one of them and then apply the same results to the other.

Furthermore, knowing [16] that $\mathbf{C}^T = \mathbf{C}$ and, similarly, $\mathbf{S}^T = \mathbf{S}$, we can get the following relation: $\mathbf{A}^{-1}\mathbf{C} = \mathbf{C}\mathbf{A}^{-1^T}$. Using this result in the above equations, we find that

$$\mathbf{A}^{-1\dagger}(\mathbf{D}\mathbf{A}^{-1^T}-\mathbf{S}^\dagger \mathbf{D}\mathbf{A}^{-1}\mathbf{C})\frac{\partial \mathbf{S}}{\partial \rho}\mathbf{A}^{-1}$$
$$= \mathbf{A}^{-1\dagger}(\mathbf{D}-\mathbf{S}^\dagger \mathbf{D}\mathbf{C})\mathbf{A}^{-1^T}\frac{\partial \mathbf{S}}{\partial \rho}\mathbf{A}^{-1}. \tag{B6}$$

Next, we define the $\mathbf{S}_{\text{cell}}$ matrix (the scattering matrix for a single cell of the TL mesh):

$$\mathbf{S}_{\text{cell}} = (\mathbf{I}+R\mathbf{S}_0)^{-1}(\mathbf{S}_0+R\mathbf{I}), \tag{B7}$$

where $R = (Z_0-1)/(Z_0+1)$ (scalar) and $\mathbf{S}_0 = (\frac{1}{2}\mathbf{U}-\mathbf{I})e^{-\beta_0 d(\alpha\pm i)}$, is the S-matrix of the TL crossing, where the plus sign corresponds to the DPS cells and the minus sign is for the DNG cells; and $\alpha = \alpha_{\text{DPS}}$ or $\alpha = \alpha_{\text{DNG}}$ is the relative loss parameter for the respective cells, and $i = \sqrt{-1}$ is the imaginary unit. Here, $\mathbf{U}$ represents a 4×4 matrix with all components equal to unity and $\mathbf{I}$ is the 4×4 identity matrix.

Starting with the Z_0 parameter, we can write

$$\frac{\partial \mathbf{S}_{\text{cell}}}{\partial Z_0} = -(\mathbf{I}+R\mathbf{S}_0)^{-1}\frac{dR}{dZ_0}(\mathbf{S}_0(\mathbf{I}+R\mathbf{S}_0)^{-1}(\mathbf{S}_0+R\mathbf{I})-\mathbf{I})$$
$$= -(\mathbf{I}+R\mathbf{S}_0)^{-1}\frac{dR}{dZ_0}(\mathbf{S}_0\mathbf{S}_{\text{cell}}-\mathbf{I}). \tag{B8}$$

By using the result $dR/dZ_0 = 2(Z_0+1)^{-2}$, we get the following formula for the derivative,

$$\frac{\partial \mathbf{S}_{\text{cell}}}{\partial Z_0} = -\frac{2}{(Z_0+1)^2}(\mathbf{I}+R\mathbf{S}_0)^{-1}(\mathbf{S}_0\mathbf{S}_{\text{cell}}-\mathbf{I}). \tag{B9}$$

Performing the same steps for the $\beta_0 d$ parameter, we obtain the following relation,

$$\frac{\partial \mathbf{S}_{\text{cell}}}{\partial(\beta_0 d)} = (\mathbf{I}+R\mathbf{S}_0)^{-1}\frac{d\mathbf{S}_0}{d(\beta_0 d)}[\mathbf{I}-R(\mathbf{I}+R\mathbf{S}_0)^{-1}(\mathbf{S}_0+R\mathbf{I})]$$
$$= (\mathbf{I}+R\mathbf{S}_0)^{-1}\frac{d\mathbf{S}_0}{d(\beta_0 d)}(\mathbf{I}-R\mathbf{S}_{\text{cell}}). \tag{B10}$$

Finally, by noting that $d\mathbf{S}_0/d(\beta_0 d) = -(\alpha \pm i)\mathbf{S}_0$, we can reduce this equation to

$$\frac{\partial \mathbf{S}_{\text{cell}}}{\partial(\beta_0 d)} = -(\alpha \pm i)(\mathbf{I}+R\mathbf{S}_0)^{-1}\mathbf{S}_0(\mathbf{I}-R\mathbf{S}_{\text{cell}}). \tag{B11}$$

APPENDIX C: ALGORITHMS

Here we present the algorithms for the three optimization strategies used in this work. The following common notations are used: r is the ring index; N is the total number of rings; M and L are the maximum numbers of iterations in i and j, respectively; $\{\beta_0 d, Z_0\}$ denotes the whole sequence (or vector) of the optimization parameters; SIMULATION () is the FDTLM-based procedure that calculates the absorption cross section σ_{abs} (and its gradient $\nabla \sigma_{\text{abs}}$) for a metamaterial wormhole object with the given set of parameters; APPEND (*elem*, *seq*) appends an element *elem* to the sequence *seq*; REPLACE (*n*, *seq*, *elem*) returns a sequence with the *n*th element of *seq* replaced by *elem*.

Algorithm 1. Ring-by-ring algorithm.

---

function RINGBYRING(N)
  $sol \leftarrow \{\}$ ▷ Start with empty sequence
  for $r \leftarrow 1, 2, \ldots N$ **do**   ▷ Loop for N rings
    $max \leftarrow 0$
    for $b \leftarrow 0.01, \ldots 1.0$ **do**
      for $z \leftarrow 0.01, \ldots 5.0$ **do**
        $\{\beta_0 d, Z_0\} \leftarrow$ APPEND($(b, z), sol$)
        $\sigma_{\text{abs}} \leftarrow$ SIMULATION($\{\beta_0 d, Z_0\}$)
        if $\sigma_{\text{abs}} > max$ **then**
          $max \leftarrow \sigma_{\text{abs}}$
          $sol \leftarrow \{\beta_0 d, Z_0\}$
        end if
      end for
    end for
  end for
  return max, sol ▷ Return optimal $\sigma_{\text{abs}}(\beta_0 d, Z_0)$
end function

Algorithm 2. Gradient descent algorithm.

---

function GRADIENTDESCENT($N, \{\beta_0^{\text{in}}d, Z_0^{\text{in}}\}, M, \kappa, \gamma$)
  $v \leftarrow 0$
  $max \leftarrow 0$
  $\{\beta_0 d, Z_0\} \leftarrow \{\beta_0^{\text{in}}d, Z_0^{\text{in}}\}$ ▷ Initial params for N rings
  for $i \leftarrow 1, 2, \ldots M$ **do**
    $(\sigma_{\text{abs}}, \nabla \sigma_{\text{abs}}) \leftarrow$ SIMULATION($\{\beta_0 d, Z_0\}$)
    $v \leftarrow (1-\gamma)v + \kappa \nabla \sigma_{\text{abs}}$
    $\{\beta_0 d, Z_0\} \leftarrow \{\beta_0 d, Z_0\} + v$
    if $\sigma_{\text{abs}} > max$ **then**
      $max \leftarrow \sigma_{\text{abs}}$
      $sol \leftarrow \{\beta_0 d, Z_0\}$
    end if
    if $v = 0$ **then break**
  end for
  return max, sol ▷ Return optimal $\sigma_{\text{abs}}(\beta_0 d, Z_0)$
end function

Algorithm 3. Mixed algorithm.

```
function MIXEDGRADIENT(N, {β₀ⁱⁿd}, {Z₀ⁱⁿ}, M, L)
    ν ← 0; max ← 0
    bsol ← {β₀ⁱⁿd}; zsol ← {Z₀ⁱⁿ}                              ▷ Initial set for N rings
    for i ← 1, 2, … M do
        {Z₀} ← zsol
        for j ← 1, 2, … L do                                   ▷ Z₀ optimization loop
            (σₐᵦₛ, ∇σₐᵦₛ) ← SIMULATION({bsol, Z₀})
            ν ← (1 − γ)ν + κ∇σₐᵦₛ,Z₀
            {Z₀} ← {Z₀} + ν
            if σₐᵦₛ > max then
                max ← σₐᵦₛ; zsol ← {Z₀}
            end if
            if ν = 0 then break
        end for
        for r ← 1, 2, … N do                                   ▷ β₀d optimization loop
            {β₀d} ← bsol
            for b ← 0.01, … 1 do
                {β₀d} ← REPLACE(r, {β₀d}, b)
                (σₐᵦₛ, ∇σₐᵦₛ) ← SIMULATION({β₀d, zsol})
                if σₐᵦₛ > max then
                    max ← σₐᵦₛ; bsol ← {β₀d}
                end if
            end for
        end for
    end for
    return max, bsol, zsol                                     ▷ Return optimal σₐᵦₛ(β₀d, Z₀)
end function
```

[1] C. F. Bohren and D. R. Huffman, *Absorption and Scattering of Light by Small Particles* (Wiley-VCH Verlag GmbH & Co. KGaA, Weinheim, 2007).

[2] S. Tretyakov, Plasmonics **9**, 935 (2014).

[3] M. I. Tribelsky and B. S. Lyk'yanchuk, Phys. Rev. Lett. **97**, 263902 (2006).

[4] Z. Ruan and S. Fan, Phys. Rev. Lett. **105**, 013901 (2010).

[5] M. I. Tribelsky, Europhys. Lett. **94**, 14004 (2011).

[6] Z. Ruan and S. Fan, Appl. Phys. Lett. **98**, 043101 (2011).

[7] X. Fan, W. Zheng, and D. J. Singh, Light: Sci. Appl. **3**, e179 (2014).

[8] N. Mohammadi Estakhri and A. Alù, Phys. Rev. B **89**, 121416(R) (2014).

[9] A. E. Miroshnichenko and M. I. Tribelsky, Phys. Rev. Lett. **120**, 033902 (2018).

[10] J. Ng, H. Chen, and C. T. Chan, Opt. Lett. **34**, 644 (2009).

[11] C. A. Valagiannopoulos, J. Vehmas, C. R. Simovski, S. A. Tretyakov, and S. I. Maslovski, Phys. Rev. B **92**, 245402 (2015).

[12] S. Maslovski, C. Simovski, and S. Tretyakov, New J. Phys. **18**, 013034 (2016).

[13] S. I. Maslovski, C. R. Simovski, and S. A. Tretyakov, in *Proceedings of SPIE, Metamaterials X*, edited by A. D. Boardman *et al.* (SPIE, Bellingham, WA, 2016), Vol. 9883, p. 98830O.

[14] W. J. Padilla, D. N. Basov, and D. R. Smith, MaterialsToday **9**, 28 (2006).

[15] S. Maslovski, in *Proceedings of the 10th International Congress on Advanced Electromagnetic Materials in Microwaves and Optics (METAMATERIALS)* (IEEE Xplore, Piscataway, NJ, 2016), p. 220.

[16] S. I. Maslovski, H. R. L. Ferreira, I. O. Medvedev, and N. G. B. Brás, Phys. Rev. B **98**, 245143 (2018).

[17] V. G. Veselago, Sov. Phys. Usp. **10**, 509 (1968).

[18] G. V. Eleftheriades, MaterialsToday **12**, 30 (2009).

[19] P. Alitalo, S. Maslovski, and S. Tretyakov, J. Appl. Phys. **99**, 064912 (2006).

[20] P. Alitalo, S. Maslovski, and S. Tretyakov, J. Appl. Phys. **99**, 124910 (2006).

[21] E. E. Narimanov and A. V. Kildishev, Appl. Phys. Lett. **95**, 041106 (2009).

[22] Q. Cheng, T. J. Cui, W. X. Jiang, and B. G. Cai, New J. Phys. **12**, 063006 (2010).

[23] H. Chen, R.-X. Miao, and M. Li, Opt. Express **18**, 15183 (2010).

[24] Y. Yang, L. Y. Leng, N. Wang, Y. Ma, and C. K. Ong, J. Opt. Soc. Am. A **29**, 473 (2012).

[25] J. B. Pendry, D. Schurig, and D. R. Smith, Science **312**, 1780 (2006).

[26] H. Jin and R. Vahldieck, IEEE Trans. Microwave Theory Tech. **20**, 2207 (1992).

[27] C. Christopoulos, *The Transmission-Line Modeling Method in Electromagnetics*, Synthesis Lectures on Computational

Electromagnetics No. 7 (Morgan & Claypool Publishers, San Rafael, CA, 2006).

[28] J. W. Demmel, S. C. Eisenstat, J. R. Gilbert, X. S. Li, and J. W. H. Liu, SIAM J. Matrix Anal. Appl. **20** 720 (1999).

[29] X. S. Li, J. W. Demmel, J. R. Gilbert, L. Grigori, P. Sao, M. Shao, and I. Yamazaki, *Tech report LBNL-44289: SuperLU User's Guide* (Lawrence Berkeley National Laboratory, Berkeley, CA, 1999). Retrieved from https://portal.nersc.gov/project/sparse/superlu/.